



Research paper

Practical identification approach for the actuation dynamics of autonomous surface vehicles with minimal instrumentation

Thalia Morel ^{a,*,} Luis Orihuela ^{b,c,} Christophe Combastel ^{d,} Guillermo Bejarano ^{a,}

^a Department of Engineering, Universidad Loyola Andalucía, Avenida de las Universidades, 2, 41704, Dos Hermanas (Seville), Spain

^b Dept. Ingeniería Electrónica, Sistemas Informáticos y Automática, Universidad de Huelva, Avda. de las Fuerzas Armadas, S/N, 21007, Huelva, Spain

^c Centro de Investigación en Tecnología, Energía y Sostenibilidad, Universidad de Huelva, Ctra. Huelva-Palos de la Frontera, Campus La Rábida, 21819, Palos de la Frontera (Huelva), Spain

^d Univ. Bordeaux, CNRS, Bordeaux INP, IMS, UMR 5218, F-33400, Talence, France

ARTICLE INFO

MSC:

93B30

93C10

Keywords:

Autonomous surface vehicles

System identification

Actuation modelling

Inertia

Vessel dynamics

ABSTRACT

A practical method for identifying the propeller model and inertia matrix of a marine Autonomous Surface Vehicle (ASV) is proposed in this work. Special attention is paid to limiting the instrumentation requirements. Based on a generic grey-box dynamic modelling addressing the considered catamaran-shaped ASV architecture, the static/dynamic behaviour of both propellers and the vessel dynamic are jointly estimated using the sole measurements of position, heading, and propellers pulse width modulation (PWM) signals. No accelerometer is required. Two distinct grey-box configurations involving either a static polynomial or a dynamic modelling of each propeller are proposed and compared. The resulting ASV identification methodology is shown to provide insight into the whole vessel inertial characteristics, which are key enablers in the development of autonomous navigation and control systems. Model validation was performed using data collected from the reported experiments. Model prediction errors related to both linear velocities and yaw rate are evaluated and compared based on given metrics. The results underscore the robustness and accuracy of the identified models in capturing the essential dynamics of the ASV, with a determination coefficient that consistently exceeds 0.94 for all estimated velocities.

1. Introduction

Recent advances in ASVs have opened up new and exciting possibilities in various applications, offering a potential reduction in the reliance on large manned ships that cause high operational costs (Jovanović et al., 2024; Gantiva Osorio et al., 2024). These autonomous vehicles have the ability to revolutionise several fields, including search and rescue operations, ocean exploration/monitoring, border surveillance, maritime security among other civilian and military applications. Using ASVs, these tasks can be performed efficiently, leading to improved safety, cost savings, and improved environmental stewardship (Morel et al., 2022a; Gantiva Osorio et al., 2024).

ASVs have gained significant attention for both research and civil applications since the early 1990s (Simetti and Indiveri, 2022). Notable prototypes include the catamaran *AutoCat* for the collection of hydrographic data (Wu et al., 2022), the autonomous kayak *SCOUT* for acoustic navigation and autonomous system tests (Curcio et al., 2005), and the *Measuring Dolphin* of the University of Rostock for water monitoring (Majohr and Buch, 2006). Other examples include the *Charlie* catamaran from CNR-ISSIA for sea surface sampling (Caccia

et al., 2007) and the *Delfim* from IST-ISR for enhancing acoustic communication (Alves et al., 2006).

With a similar purpose of water body monitoring and pollution tracking, an autonomous catamaran-like surface vessel named *Yellowfish* has been conceived and developed at Universidad Loyola Andalucía. This vessel is designed to navigate through calm water and at low speed, due to its size and the power of its actuation system, while relying on a minimal instrumentation scheme.

Motion control is crucial to ensure safe navigation and successful path following of the ASV, despite the significant effect of non-measured disturbances due to wind, waves, and currents in real environments (Breivik, 2010). Most control design strategies presented in the literature rely on an open-loop dynamic model of the vessel behaviour including its actuation system. However, obtaining an accurate model for an ASV based on physical principles can be challenging due to strong non-linearities, unmodelled hydrodynamics related to neglected degrees of freedom, environmental disturbances, and internal parametric uncertainty. However, modelling and identifying such

* Corresponding author.

E-mail address: tamorel@uloyola.es (T. Morel).

<https://doi.org/10.1016/j.oceaneng.2024.120098>

Received 24 August 2024; Received in revised form 11 October 2024; Accepted 10 December 2024

0029-8018/© 2024 Elsevier Ltd. All rights are reserved, including those for text and data mining, AI training, and similar technologies.

systems remain essential for accurate navigation and control of the vessel (Peng et al., 2020). Conventional approaches often require extensive instrumentation, including acceleration measurements, which may increase both the cost and complexity of the system.

Several experimental works in the literature have addressed the identification of dynamic models for the motion of different kinds of ASVs. In the literature, the works analysed in the following differ in their approach, objectives and layout of the vehicles considered, and they give insight into the current state of the art. This contributes to highlight the main techniques used, as well as some of their main restrictions to jointly identify both the ASV dynamics and actuation system.

Sonnenburg and Woolsey (Eriksen and Breivik, 2017) developed a planar motion model for a single-hull ASV, comparing experimentally identified models under different speeds and conditions, using a modified rigid-hull inflatable boat Sonnenburg and Woolsey (2013). Their multiple-model approach adjusts based on nominal speed. This paper proposes a control-oriented modelling procedure for a high-speed rigid-hull inflatable ASV across various speed regions, without explicitly modelling the actuation system.

Wu et al. proposed a method to identify linear and non-linear hydrodynamic coefficients using a Support Vector Machine (SVM) (Wu et al., 2022) for the modelling of ASV manoeuvres. Linear coefficients were identified from turning tests at small water-jet angles, while larger angles and the linear coefficients were used for non-linear coefficient identification. The model accurately describes the manoeuvrability of the ASV. Xu et al. combined the Least Square Support Vector Machine (LSSVM) with the Cuckoo Search (CS) algorithm to identify a 3-DOF dynamic model of an ASV (Xu et al., 2020), outperforming other methods to predict surge and sway velocities, although accurate velocity measurements are required.

In Abrougui et al. (2021), a 3-DOF control-oriented dynamic model for an ASV was proposed, with parameters determined through theoretical and experimental methods. The control system enables the ASV to follow a desired trajectory accurately, leading to the conclusion that lateral sway is negligible in closed-loop control. The emphasis is on achieving sufficient accuracy for motion control rather than precise parameter estimation.

Caccia et al. proposed a least-squares identification procedure for ASVs using basic sensors onboard that are typically found in small, low-cost vessels (Caccia et al., 2008). Validation was performed using data from auto-heading and line-following manoeuvres in typical conditions. Linear and quadratic models were applied to the propellers in the actuation system. The linear drag model performed better at low angular rates but overestimated yaw rates at high rudder angles, unlike the quadratic model.

Simetti and Indiveri recently proposed a first-principle manoeuvring model for a small twin-thruster ASV, addressing non-linearity and asymmetry due to the catamaran layout's unequal port/starboard dynamics (Simetti and Indiveri, 2022). The model adapts hydrodynamic derivatives for large or tight turns and is identified by correlating constant thruster revolutions per minute (RPM) with steady-state surge and yaw rates from the Global Navigation Satellite System (GNSS) and inertial data. They propose identifying both the ASV's dynamic and actuation models concurrently, but sway dynamics are not identified, and the damping matrix is assumed to be diagonal.

As a summary of the literature review, despite the different approaches, focus, and ASV layouts, three main facts appear:

- Previous works address either the identification of the dynamic model of the vessel, or the actuation model, but not the combined effect on the vehicle motion, at least without strong assumptions on the model structure or the availability of accurate velocity measurements.
- Those works that focus on the identification of simplified control-oriented dynamic models sacrifice, in most cases, the identification of individual parameters of the model.

- Concerning the description of the actuation system, both linear and quadratic static models have been considered. Dynamic effects are omitted in most cases.

In this work, a practical identification approach is proposed to obtain a control-oriented dynamic model of an ASV with limited instrumentation. Reported *Yellowfish* operations provided the experimental data sets (made available) used to validate the proposed methodology. It focuses on the identification of the so-called *input gain* term (Peng et al., 2021), which relates the PWM signals applied to the propellers to the accelerations generated in the vessel, thus merging the actuation system with the inertial properties of the vessel. This term turns out to be key for motion control and state estimation (Abrougui et al., 2021; Peng et al., 2021). In this context, the main contribution of the paper consists in proposing an original grey-box modelling approach involving polynomial and dynamic terms to accurately identify this so-called *input gain*, based on a minimal instrumentation scheme. The comparison and experimental validation of the resulting models are shown to provide valuable insights not only into the characteristics of both the propellers and the inertia matrix but also into the whole ASV dynamic.

The paper is organised as follows. After this introduction, the problem is stated in Section 2. Section 3 describes the experimental platform, detailing the *Yellowfish* ASV with the instrumentation used and the available data. Section 4 details the models considered for both the vessel dynamics and the actuation system. Then, Section 5 describes the proposed identification procedure for all actuation models considered. Section 6 describes the experimental results, presents the obtained models, and reports the validation results. It also discusses model selection, considering the uncertainty in identifying model coefficients. Finally, concluding remarks are given in Section 7.

2. Problem statement

In order to state the ASV grey-box modelling and identification problem addressed in this work, the kinematics and kinetics of a surface vessel in horizontal motion are first described using the following dynamic model (Fossen, 2011):

$$\begin{cases} \dot{\eta} = R(\psi)v \\ M\dot{v} = -C(v)v - D(v)v - g(\eta) + \tau_w + \tau, \end{cases} \quad (1)$$

where $\eta = [x \ y \ \psi]^T$ is the planar position and heading vector expressed in the earth-fixed inertial frame $\{n\}$ (see Fig. 1), $v = [u \ v \ r]^T$ is the linear and angular velocity vector expressed in the body-fixed frame $\{b\}$, $\tau = [F_u \ F_v \ \tau_r]^T$ refers to the force/torque vector, which represents the control action, and $\tau_w = [F_{w,u} \ F_{w,v} \ \tau_{w,r}]^T$ refers to the environmental forces and torque due to wind, waves, and currents. M is the inertia matrix, $C(v)$ the Coriolis and centrifugal matrix, $D(v)$ the damping matrix, and $g(\eta)$ describes the gravitational and buoyancy forces, which are neglected for a surface vehicle in planar movements. Note that an underactuated actuation system is considered, i.e. $\tau = [F_u \ 0 \ \tau_r]^T$, since there is no lateral force in τ .

As first stated in Liu et al. (2019), the lumped generalised disturbance vector $\sigma = [\sigma_u \ \sigma_v \ \sigma_r]^T \in \mathbb{R}^3$ can be defined as:

$$\sigma \equiv M^{-1}(-C(v)v - D(v)v - g(\eta) + \tau_w). \quad (2)$$

Vector σ groups together disturbances due to hydrodynamic effects, internal unmodelled and coupling dynamics, uncertainties, and external disturbances. Using (2), the body dynamic model (1) can be redefined as:

$$\begin{cases} \dot{\eta} = R(\psi)v, \\ \dot{v} = M^{-1}\tau + \sigma. \end{cases} \quad (3)$$

The so-called input gain $G = [G_u \ G_v \ G_r]^T \in \mathbb{R}^3$ is then defined as:

$$G \equiv M^{-1}\tau, \quad (4)$$

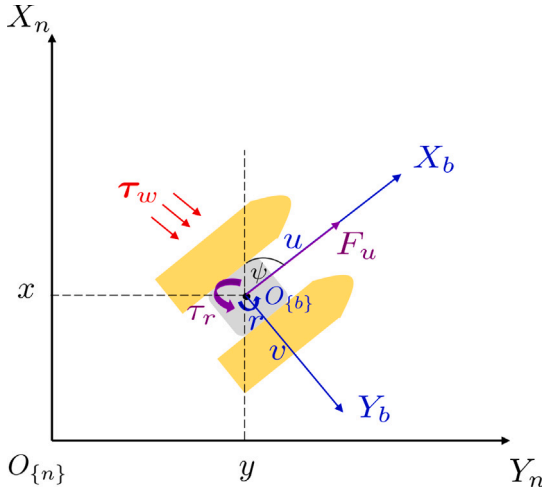


Fig. 1. Reference frames of the vessel.

and depends on both the vessel inertial characteristics and the truly applied propelling force and torque. Though the latter are closely related to the propellers' PWM control signals (denoted as δ_L and δ_R for the left and right propeller, respectively), the corresponding relation $G(\delta_L, \delta_R)$ is most often far from trivial. In fact, it may feature nonlinear and dynamic effects, including possible switching related to propellers' forward and reverse modes. Moreover, a simple characterisation from first physical principles (knowledge model) cannot be easily derived from the sole propeller characteristics since the truly applied propelling force and torque depend not only on the position of propellers on the vessel but also on much more complex and possibly coupled hydrodynamics phenomena. This motivates the development of an identification methodology primarily focused on the estimation of $G(\delta_L, \delta_R)$ from experimental data.

More precisely, the aim of this work is,

- firstly, to define and compare relevant grey-box models (non-linear, dynamic) for the so-called input gain $G = G(\delta_L, \delta_R)$ in (4),
- then estimate all related parameters and,
- finally, validate the resulting whole ASV dynamic model based on explicitly given metrics.

Another requirement of the identification methodology is to rely on a minimal instrumentation scheme reduced to the linear position measurements given by the GNSS system, the heading measured by the Attitude and Heading Reference Systems (AHRS), and the propellers' PWM control signals. Such signals are easily made available for a wide class of ASVs, including the catamaran-shaped *YellowFish* described in Section 3 and serving as an illustrative application case in this paper.

3. Experimental platform, instrumentation and available data

The *Yellowfish* ASV, depicted in Fig. 2, is a catamaran vessel made of fibreglass, measuring 128 cm long and 98 cm wide. The catamaran design features two identical hulls, firmly connected by aluminium bars. The propulsion of the *Yellowfish* ASV is provided by two T200 thrusters manufactured by BlueRobotics, which are electric propeller motors.

Regarding hardware, the ASV features a Raspberry Pi 4 model B integrated with a Navio2 for command and data processing. The Raspberry Pi 4, a mini-computer, operates with an integrated system specifically tailored to align with the characteristics of Navio2. Its primary role within the system is to facilitate telemetry support. The experimental platform, equipped with the necessary sensors and hardware for data acquisition, is shown in Fig. 2.

Furthermore, the software implemented on the Navio2 is called Ardupilot. Essentially, Navio2 uses Ardupilot for comprehensive sensor configuration and vehicle control across all installed vehicles. Mission Planner serves as the ground station software utilised for telecommunication purposes with the ship. The DataFlash logs can be obtained through Mavlink from the Mission Planner and create a MATLAB file with all sensor values. For additional details on the *Yellowfish* ASV's hardware and software, the reader is referred to Morel et al. (2022b, 2023).

The *Yellowfish* ASV mounts different sensors whose available data and their respective sampling times are presented in Table 1. As seen in the table, the sensors have different sampling times: The AHRS at 20 ms and the GNSS at 200 ms. In addition to these outputs, the PWM signals generated with the radio controller (RCOU) can be measured with a sampling time of 100 ms.

Based on the data provided by the mentioned sensors, some transformations are necessary to obtain the variables used in the vessel model. First, each propeller (left and right) takes a PWM signal as input. The PWM values of the left and right thrusters are normalised between $[-1, 1]$. This signal, after normalisation, can be described by $\delta_i \in [-1, 1]$, $i \in \{L, R\}$, being $\delta_i = \pm 1$ a PWM signal with a duty cycle of 100%, and $\delta_i = 0$ a PWM signal with a duty cycle of 0%. More details on the normalisation of the PWM signals can be found in Morel et al. (2022b). The propellers produce forward motion forces for positive values of δ_i . Other metrics, such as planar positioning coordinates $\{x, y\}$, are obtained by transforming point locations provided by the GNSS from geographic coordinates to local Cartesian coordinates, returned as north-east-down (NED). After this transformation, a location shift is performed, as the GNSS antenna is not positioned at the same place as the Navio2, from which other data are derived. The heading ψ is measured directly by the AHRS.

4. Modelling

This section aims to find the expression for the input gain as a grey-box model, requiring the complete modelling of the vehicle. The overall vehicle model is represented by the block diagram in Fig. 3, where the system is divided into two primary components: the actuation system and the ASV body. The actuation system takes the PWM signals for the left and right propellers, denoted as δ_L and δ_R , as inputs. It then produces the force F_u and the torque τ_r applied to the vessel body as outputs, using thrusts T_L and T_R as intermediate variables within the actuation system. The ASV body takes the force F_u and torque τ_r as inputs and produces, as outputs, the full state of the vessel, consisting of its 3-DOF position η and velocity v vectors. In the following subsections, further details are given for the models of each block.

4.1. ASV body

Based on the kinetic equation presented in (3), considering manoeuvring theory (almost constant positive forward speed and relatively calm water) and assuming homogeneous mass distribution and $X_b - Z_b$ -plane symmetry, being X_b and Z_b the aft-to-fore and top-to-bottom axes, respectively (see Fossen (2011)), the structure of M is shown in (5):

$$M = \begin{bmatrix} m - X_{\dot{u}} & 0 & 0 \\ 0 & m - Y_{\dot{v}} & mx_g - Y_{\dot{r}} \\ 0 & mx_g - Y_{\dot{r}} & I_z - N_{\dot{r}} \end{bmatrix}, \quad (5)$$

where m is the ASV total mass, x_g is the distance from the centre of gravity of the vessel to the origin of $\{b\}$ (measured along X_b), I_z is the moment of inertia about the Z_b axis, and $X_{(\cdot)}$, $Y_{(\cdot)}$, and $N_{(\cdot)}$ are hydrodynamic parameters according to standard notation (The Society of Naval Architecture and Marine Engineers, 1950). Notice that $M =$

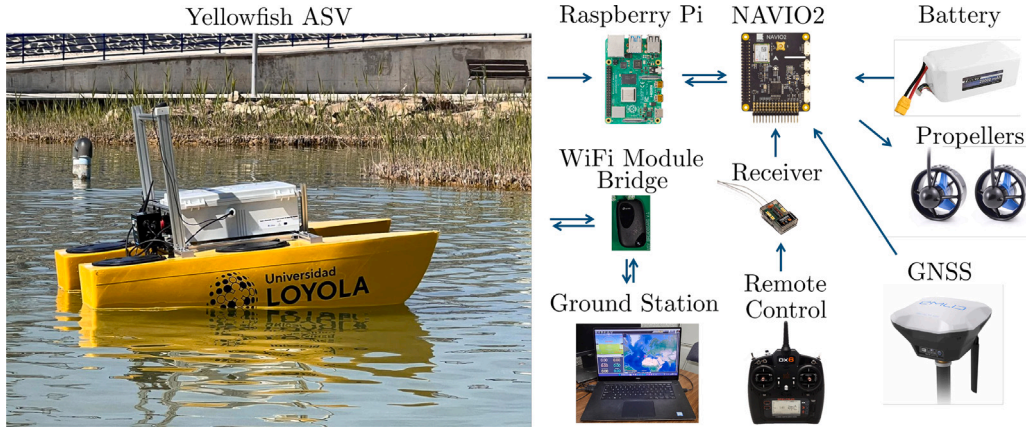


Fig. 2. The Yellowfish ASV experimental platform.

Table 1

Summary of sensor data and variables for vessel model analysis.

Sensor	Available data	Sampling rate	Obtained variable	Unit	Description of variable
GNSS	Latitude, longitude	200 ms	x, y	m	North and east absolute position
RCOU	PWM _L , PWM _R	100 ms	δ_L, δ_R	μs	Propellers normalised duty cycle
AHRS	Heading	20 ms	ψ	rad	Heading angle

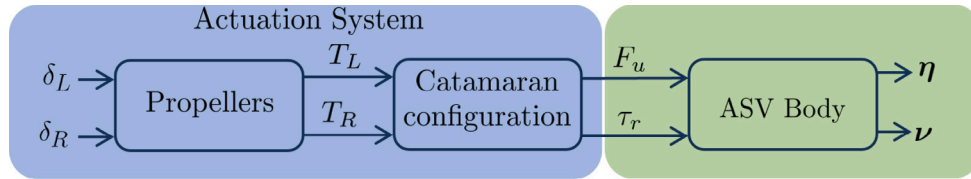


Fig. 3. Block diagram of the ASV, highlighting the actuation system and the ASV body.

M^T , and the structure of M ensures that M^{-1} exists for well-designed vessels (Fossen, 2011).

According to Fossen (2011), Coriolis $C(v)$ and damping $D(v)$ matrices are given by:

$$C(v) = \begin{bmatrix} 0 & 0 & -(m - Y_v)v - (m x_g - Y_r)r \\ 0 & 0 & (m - X_u)u \\ (m - Y_v)v + (m x_g - Y_r)r & -(m - X_u)u & 0 \end{bmatrix}, \quad (6)$$

$$D(v) = \begin{bmatrix} -X_u - X_{|u|}|u| & 0 & 0 \\ 0 & -Y_v - Y_{|v|}|v| - Y_{|r|}|r| & -Y_r - Y_{|v|}|v| - Y_{|r|}|r| \\ 0 & -N_v - N_{|v|}|v| - N_{|r|}|r| & -N_r - N_{|v|}|v| - N_{|r|}|r| \end{bmatrix}. \quad (7)$$

Note that the damping matrix considers non-linear terms, which are neglected in most identification papers but which will be kept in this work.

The rotation matrix $R(\psi)$ between $\{b\}$ and $\{n\}$ is given by:

$$R(\psi) = \begin{bmatrix} \cos(\psi) & -\sin(\psi) & 0 \\ \sin(\psi) & \cos(\psi) & 0 \\ 0 & 0 & 1 \end{bmatrix} = \begin{bmatrix} R_2(\psi) & \mathbf{0} \\ \mathbf{0} & 1 \end{bmatrix}, \quad (8)$$

where $R_2(\psi) \in \mathbb{R}^{2 \times 2}$ is the upper left submatrix of $R(\psi)$.

In this study, the identification process relies on a discretised version of the kinetics equation, chosen for the incorporation of unknown disturbances. The discrete-time kinetics equation is then derived, with h denoting the sampling period, as follows:

$$v(k+1) = v(k) + hM^{-1}\tau(k) + h\sigma(k). \quad (9)$$

More precisely, the discretised system dynamics presented in (9) can be divided into three equations, corresponding to every velocity component, as shown:

$$\begin{aligned} u(k+1) &= u(k) + hM^{-1}(1,1)F_u(k) + h\sigma_u(k), \\ v(k+1) &= v(k) + hM^{-1}(2,3)\tau_r(k) + h\sigma_v(k), \\ r(k+1) &= r(k) + hM^{-1}(3,3)\tau_r(k) + h\sigma_r(k), \end{aligned} \quad (10)$$

where $M^{-1}(i,j)$ stands for the (i,j) element of the inverse of the inertia matrix. Then, it is evident that the input gains can be mathematically defined as:

$$\begin{aligned} G_u(k) &:= hM^{-1}(1,1)F_u(k), \\ G_v(k) &:= hM^{-1}(2,3)\tau_r(k), \\ G_r(k) &:= hM^{-1}(3,3)\tau_r(k). \end{aligned} \quad (11)$$

From (2), it can be assumed that each of the components of σ can be approximated as a quasi-quadratic function of v plus some disturbances:

$$\sigma_j = v^T P_j |v| + v^T Q_j v + R_j v + c_j, \quad (12)$$

where $j \in \{u, v, r\}$, $P_j \in \mathbb{R}^{3 \times 3}$, $R_j \in \mathbb{R}^{1 \times 3}$, and $Q_j \in \mathbb{R}^{3 \times 3}$ are constant matrices assumed to be symmetric, and $c_j \in \mathbb{R}$ is a possible time-varying vector accounting for the effect of wind, waves, and currents. In particular:

$$\begin{aligned} P_u &= \begin{bmatrix} P_u^{(1,1)} & 0 & 0 \\ 0 & 0 & 0 \\ 0 & 0 & 0 \end{bmatrix}, \quad Q_u = \begin{bmatrix} 0 & 0 & 0 \\ 0 & 0 & Q_u^{(2,3)} \\ 0 & Q_u^{(2,3)} & Q_u^{(3,3)} \end{bmatrix}, \quad R_u = \begin{bmatrix} R_u^{(1)} & 0 & 0 \end{bmatrix} \\ P_v &= \begin{bmatrix} 0 & 0 & 0 \\ 0 & P_v^{(2,2)} & P_v^{(2,3)} \\ 0 & P_v^{(3,2)} & P_v^{(3,3)} \end{bmatrix}, \quad Q_v = \begin{bmatrix} 0 & Q_v^{(1,2)} & Q_v^{(1,3)} \\ Q_v^{(1,2)} & 0 & 0 \\ Q_v^{(1,3)} & 0 & 0 \end{bmatrix}, \end{aligned}$$

$$\mathbf{R}_v = \begin{bmatrix} 0 & R_v^{(2)} & R_v^{(3)} \end{bmatrix}$$

$$\mathbf{P}_r = \begin{bmatrix} 0 & 0 & 0 \\ 0 & P_r^{(2,2)} & P_r^{(2,3)} \\ 0 & P_r^{(3,2)} & P_r^{(3,3)} \end{bmatrix}, \quad \mathbf{Q}_r = \begin{bmatrix} 0 & Q_r^{(1,2)} & Q_r^{(1,3)} \\ Q_r^{(1,2)} & 0 & 0 \\ Q_r^{(1,3)} & 0 & 0 \end{bmatrix},$$

$$\mathbf{R}_r = \begin{bmatrix} 0 & R_r^{(2)} & R_r^{(3)} \end{bmatrix}$$

4.2. Actuation system

The physical actuation system comprises two parts. First, the propellers that receive individual normalised PWM signals δ_L , δ_R and generate thrusts $T_L(\delta_L)$, $T_R(\delta_R)$. This first part has received a lot of attention in the literature, as propellers have complex nonlinear dynamics and are difficult to model and identify (Simetti and Indiveri, 2022; Blanke et al., 2000; Mu et al., 1889; Zuev et al., 2020; Simmons, 2021). In the current configuration, it is reasonable to assume that both propellers are identical. Thus, a unique function $T(\delta_i)$, $i \in \{L, R\}$, is considered valid for both propellers.

The second part is the particular configuration of the vessel that allows a static transformation from the thrusts of each propeller to the force and torque received by the body. For the *Yellowfish* ASV, the force F_u and torque τ_r , expressed in the body-fixed frame $\{b\}$, can be found as:

$$F_u = T(\delta_L) + T(\delta_R), \quad \tau_r = \frac{d}{2} (T(\delta_L) - T(\delta_R)), \quad (13)$$

where d is the distance between propellers, and $T(\delta_i)$, with $i \in \{L, R\}$, represents the thrust dynamic model for any of the identical propellers.

Attending to the previous discussion, and to previous modelling in the literature, in this manuscript we have considered different models:

- Function $T(\delta_i)$ is a static quadratic function of the PWM signal applied to the propeller. Considering the thrust quadratic with the RPM is common in the literature (see, for instance, Simetti and Indiveri (2022)). Since the RPM is not a manipulable input, we seek a model that takes the PWM signal as input, assuming that this quadratic relation is preserved.
- Function $T(\delta_i)$ can be approximated by a first-order dynamic system. Again, this sort of model has been used in the literature (see, for example, Blanke et al. (2000)).

The next subsections present the aforementioned models. To simplify the notation, and assuming that both propellers are identical and thus share the same model, the subscripts $i \in \{L, R\}$ will be removed.

4.2.1. Second-order static model

The thrust $T(\delta(k))$ is assumed to be described as:

$$T(\delta(k)) = \begin{cases} a_f \delta(k)^2 + b_f \delta(k), & \delta(k) \geq 0^+ \\ a_r \delta(k)^2 + b_r \delta(k), & \delta(k) < 0^- \end{cases} \quad (14)$$

where $\delta(k) \in [-1, 1]$ is the normalised PWM signal, and $a_j, b_j \in \mathbb{R}$ with $j \in \{f, r\}$ are unknown scalars, where subindices f and r stand for forward and reverse motion, respectively. Eq. (14) establishes four regions of operations attending to the rotation of the left and right propellers. The (f, f) region will occur when the ASV moves forward in a straight line or with low-curvature trajectories. High-curvature trajectories are defined by the (f, r) and (r, f) regions. Finally, the reverse motion will be attained with the (r, r) region.

As the primary objective of this identification process refers to the motion control of the *Yellowfish* ASV, the latter configuration will not be employed during the identification experiments, as it does not align with the intended use-case scenario.

Remark 1. The T200 Thrusters present a non-symmetric dead zone around $\delta = 0$, which has been experimentally identified in Morel et al. (2022b). To account for it, (14) could be easily modified as:

$$T(\delta(k)) = \begin{cases} a_f (\delta(k) - \delta_f)^2 + b_f (\delta(k) - \delta_f), & \delta(k) \geq \delta_f \\ a_r (\delta(k) - \delta_r)^2 + b_r (\delta(k) - \delta_r), & \delta(k) \leq \delta_r, \\ 0, & \text{otherwise} \end{cases}$$

where $\delta_f > 0$ and $\delta_r < 0$ are the identified dead zone limits. The identification methods presented in the rest of this paper can be applied considering the previous model for the thrusters, or the one in (14). However, as the identified constants are very small, and trying to keep the notation as simple as possible to keep the focus on the identification, the rest of the document does not consider the dead zone.

4.2.2. First-order dynamic model

Both thrusts are assumed to be described by a first-order model, this is:

$$T(k) = \alpha T(k-1) + \beta T_{st}(k-1) \quad (15)$$

where $\alpha, \beta \in \mathbb{R}$ are constants to identify, and:

$$T_{st}(\delta(k)) = \begin{cases} a_f \delta(k)^2 + b_f \delta(k), & \delta(k) \geq 0^+ \\ a_r \delta(k)^2 + b_r \delta(k), & \delta(k) \leq 0^- \end{cases} \quad (16)$$

represents the static input thrust as a quadratic function of the PWM normalised signal.

5. Identification procedure

For the vehicle identification process, a specific procedure is followed as described in this section. First, the available data are prepared to meet the necessary requirements established in the previous section. Subsequently, the input gain for static propeller modelling is obtained. Finally, the equations are derived to identify the input gain, taking into account a dynamic model. This section provides a detailed explanation of the identification process for both propeller modelling.

According to Section 2, the problem to be addressed in the identification procedure is to find the input gains G_u , G_v , and G_r , whose mathematical expressions are defined in (11), using the available experimental information.

5.1. Data preparation

The procedure to transform raw experimental data into the values necessary for identification is detailed. Initially, as data are collected at varying sampling times, the longest duration, in this case the GNSS data with a sampling time of 200 ms, is used as a reference for the remainder. The input data are adjusted to use only previous points, with a cubic spline extrapolation applied to the latitude and longitude data from the GNSS. For the heading, which has a 20 ms sampling time, an 8th-degree spline extrapolation is employed. For PWM data, a third-order spline extrapolation is also used. Please note that this synchronisation with spline extrapolations has been done carefully to keep causality, which can be lost with interpolation methods.

The values required for identification include the linear velocities $\{u, v\}$ and the yaw rate r , as well as the values of δ_L and δ_R . However, instead of using individual PWM signals δ_L and δ_R as inputs, this manuscript proposes to use the PWM mean or $\bar{\delta} \equiv \frac{\delta_L + \delta_R}{2}$ and the PWM difference or $\Delta\delta \equiv \delta_L - \delta_R$. The reason is of a practical nature. In order to gather the necessary experimental data for the identification of the ASV, a series of experiments were conducted using a radio controller to issue commands to the propellers. Within this remote control system, two joysticks are configured to manipulate both the PWM mean and the PWM difference. It is not possible, with the radio controller, to choose the PWM values of each thruster independently. Furthermore, the PWM mean and difference signals are adequate to excite different kinds of dynamics, as will be explained later.

Table 2

Required data for vessel identification and their sources.

Data for identification	Required data	Description
u, v	x, y, ψ	These derivatives obtain body-referenced velocities, requiring heading.
$\bar{\delta}, \Delta\delta$	δ_L, δ_R	The left and right thruster values are transformed to obtain their mean and difference.
r	ψ	The yaw rate is obtained by the derivative of ψ .

The process of obtaining the linear velocities $\{u, v\}$ is based on the measured positions and heading. This transformation also involves changing the reference frame from inertial coordinates to body-referenced coordinates. Detailed equations for this transformation are provided in [Morel et al. \(2022b\)](#). Finally, these values are also filtered using a Savitzky–Golay filter. The yaw rate r is obtained by the derivative of ψ and then filtered using a Savitzky–Golay filter ([Savitzky and Golay, 1964](#)). [Table 2](#) details the measured data from which these necessary values are derived.

5.2. Input-gain identification for static propeller modelling

The left and right thrusts, $T(\delta(k))$, are assumed to be described as in [\(14\)](#). According to [\(13\)](#), now using the PWM mean $\bar{\delta}$ and difference $\Delta\delta$ values, the force F_u and the torque τ_r can be written as follows:

$$F_u(\bar{\delta}(k), \Delta\delta(k)) = (a_j^L + a_j^R) \left(\bar{\delta}(k)^2 + \frac{\Delta\delta(k)^2}{4} \right) + (a_j^L - a_j^R) \bar{\delta}(k) \Delta\delta(k) + (b_j^L + b_j^R) \bar{\delta}(k) + (b_j^L - b_j^R) \frac{\Delta\delta(k)}{2}, \quad (17)$$

$$\tau_r(\bar{\delta}(k), \Delta\delta(k)) = \frac{d}{2} \left((a_j^L - a_j^R) \left(\bar{\delta}(k)^2 + \frac{\Delta\delta(k)^2}{4} \right) + (a_j^L + a_j^R) \bar{\delta}(k) \Delta\delta(k) + (b_j^L - b_j^R) \bar{\delta}(k) + (b_j^L + b_j^R) \frac{\Delta\delta(k)}{2} \right), \quad (18)$$

where a_j^i, b_j^i with $i \in \{L, R\}, j \in \{f, r\}$ are the forward and reverse models to be identified for the propellers.

Now, for a better excitation of the surge dynamics, only those instants in the dataset in which the propellers work in the region (f, f) will be considered for identification. In addition, the external disturbances are considered constant for identification, this is, $c_u(k) = \bar{c}_u, \forall k$.

Proposition 1. *Provided that $\bar{\delta}(k)$ and $\Delta\delta(k)$ are known for every k , and the velocities $u(k), v(k), r(k)$ can be obtained from the position data as explained in [Section 5.1](#), the evolution of the surge at instant k for a quadratic static model for the propeller and operating in the region (f, f) satisfies:*

$$A_u(k)X_u = b_u(k), \quad (19)$$

where X_u represents a vector of unknown coefficients to identify:

$$X_u = h[P_u^{(1,1)} \quad 2Q_u^{(2,3)} \quad Q_u^{(3,3)} \quad R_u^{(1)} \quad \bar{c}_u \quad 2M^{-1}(1,1)a_f \quad 2M^{-1}(1,1)b_f]^T, \quad (20)$$

and $A_u(k), b_u(k)$ are a vector and a scalar, respectively, that can be computed from the dataset:

$$A_u(k) = \left[u(k)|u(k)| \quad v(k)r(k) \quad r(k)^2 \quad u(k) \quad 1 \quad \left(\bar{\delta}(k)^2 + \frac{\Delta\delta(k)^2}{4} \right) \quad \bar{\delta}(k) \right], \quad (21)$$

$$b_u(k) = u(k+1) - u(k). \quad (22)$$

Proof. While in the region (f, f) , the force in [\(17\)](#) can be simplified as:

$$F_u(\bar{\delta}(k), \Delta\delta(k)) = 2a_f \left(\bar{\delta}(k)^2 + \frac{\Delta\delta(k)^2}{4} \right) + 2b_f \bar{\delta}(k).$$

Subsequently, the dynamics of the surge for a quadratic static model for the propeller results in:

$$u(k+1) = u(k) + 2hM^{-1}(1,1)a_f \left(\bar{\delta}(k)^2 + \frac{\Delta\delta(k)^2}{4} \right) + 2hM^{-1}(1,1)b_f \bar{\delta}(k) + hP_u^{(1,1)}u(k)|u(k)| + 2hQ_u^{(2,3)}v(k)r(k) + hQ_u^{(3,3)}r(k)^2 + hR_u^{(1)}u(k) + hc_u(k).$$

Since the mean and difference PWM normalised signals are known, and the velocities can be obtained from the dataset, the previous equation reveals that the unknown coefficients appear in a linear fashion, as in [\(19\)](#). \square

Remark 2. The experiments were carried out on an artificial lake that had minimal influence from currents and waves. Concerning the wind, the experiments took place on relatively calm days. However, it is not possible to completely neglect the effect of the wind on lumped disturbances. To partially compensate for that, the identification procedure tries to capture a constant disturbance term \bar{c}_u with the intention of modelling a bias or persistent force in some direction.

Vector X_u can be approximated, for instance, via least-squares. As a result, the surge input gain $G_u(k)$ in [\(11\)](#) can be computed as a function of the mean and difference PWM normalised values:

$$G_u(k) = X_u(6) \left(\bar{\delta}(k)^2 + \frac{\Delta\delta(k)^2}{4} \right) + X_u(7) \bar{\delta}(k). \quad (23)$$

Concerning the yaw and sway dynamics, now the data belonging to regions $(f, f), (f, r), (r, f)$ will be used for identification. Despite the fact that sway and, particularly, yaw dynamics are better excited in regions $(f, r), (r, f)$ than in region (f, f) , the *Yellowfish* ASV is mainly designed to conduct path-following missions and, therefore, high-curvature trajectories will not be predominant.

Proposition 2. *Provided that $\bar{\delta}(k)$ and $\Delta\delta(k)$ are known for every k , and the velocities $u(k), v(k), r(k)$ can be obtained from the position data, the evolution of the sway and yaw at instant k for a quadratic static model for the propeller satisfy:*

$$A_v(k)X_v = b_v(k), \quad (24)$$

$$A_r(k)X_r = b_r(k), \quad (25)$$

where X_v and X_r are the vectors of unknown coefficients to identify:

$$X_v = h \left[P_v^{(2,2)} \quad P_v^{(2,3)} \quad P_v^{(3,2)} \quad P_v^{(3,3)} \quad 2Q_v^{(1,2)} \quad 2Q_v^{(1,3)} \quad R_v^{(2)} \quad R_v^{(3)} \quad \bar{c}_v \right. \\ \left. M^{-1}(2,3) \frac{d}{2}(a_j^L - a_j^R) \quad M^{-1}(2,3) \frac{d}{2}(a_j^L + a_j^R) \quad M^{-1}(2,3) \frac{d}{2}(b_j^L - b_j^R) \quad M^{-1}(2,3) \frac{d}{2}(b_j^L + b_j^R) \right]^T, \quad (26)$$

$$X_r = h \left[P_r^{(2,2)} \quad P_r^{(2,3)} \quad P_r^{(3,2)} \quad P_r^{(3,3)} \quad 2Q_r^{(1,2)} \quad 2Q_r^{(1,3)} \quad R_r^{(2)} \quad R_r^{(3)} \quad \bar{c}_r \right. \\ \left. M^{-1}(3,3) \frac{d}{2}(a_j^L - a_j^R) \quad M^{-1}(3,3) \frac{d}{2}(a_j^L + a_j^R) \quad M^{-1}(3,3) \frac{d}{2}(b_j^L - b_j^R) \quad M^{-1}(3,3) \frac{d}{2}(b_j^L + b_j^R) \right]^T, \quad (27)$$

and $A_v(k), A_r(k), b_v(k), b_r(k)$ are two pairs of vectors and scalars, respectively, that can be computed from the dataset.

Proof. To follow the step-by-step process of [Proposition 2](#), the reader is referred to [Morel et al. \(2024\)](#). \square

As before, vectors X_v, X_r can be approximated, for instance, via least-squares. Then, sway and yaw input gains can be computed from the mean and difference PWM normalised values:

$$G_p(k) = \begin{cases} X_p(11)\bar{\delta}(k)\Delta\delta(k) + X_p(13)\frac{\Delta\delta(k)}{2}, & (f, f) \\ X_p(10)\left(\bar{\delta}(k)^2 + \frac{\Delta\delta(k)^2}{4}\right) + X_p(11)\bar{\delta}(k)\Delta\delta(k) \\ \quad + X_p(12)\bar{\delta}(k) + X_p(13)\frac{\Delta\delta(k)}{2}, & (f, r) \\ -X_p(10)\left(\bar{\delta}(k)^2 + \frac{\Delta\delta(k)^2}{4}\right) + X_p(11)\bar{\delta}(k)\Delta\delta(k) \\ \quad - X_p(12)\bar{\delta}(k) + X_p(13)\frac{\Delta\delta(k)}{2}, & (r, f) \end{cases} \quad (28)$$

where $p \in \{v, r\}$.

Remark 3. Please note that, even though it is not the objective of the method, the previous procedure allows for a reconstruction of the lumped disturbances as a function of the velocities. This could be interesting when designing a feedforward controller that could partially compensate for the effect of such disturbances.

5.3. Input-gain identification for dynamic propeller modelling

In the process of identifying the input gain considering the dynamic propeller modelling, (15) is used for the first-order dynamic model. Following this, the procedure to obtain the regressors bears a resemblance to the approach used to identify the input gain for static propeller modelling and, hence, some developments will be simplified. The following aims to highlight the specific adaptations necessary for dynamic analysis.

Proposition 3. *Provided that $\bar{\delta}(k)$ and $\Delta\delta(k)$ are known for every k , and the velocities $u(k), v(k), r(k)$ can be obtained from the position data, the evolution of the velocities at instant k for a quadratic dynamic model for the propeller satisfies:*

$$A_{dyn,u}(k)X_{dyn,u} = b_{dyn,u}(k), \quad (29)$$

$$A_{dyn,v}(k)X_{dyn,v} = b_{dyn,v}(k), \quad (30)$$

$$A_{dyn,r}(k)X_{dyn,r} = b_{dyn,r}(k), \quad (31)$$

where $X_{dyn,u}, X_{dyn,v}$ and $X_{dyn,r}$ are the vectors of unknown coefficients to identify:

$$X_{dyn,u} = \begin{bmatrix} (\alpha + hR_u^{(1)}) & -\alpha hP_u^{(1,1)} & -\alpha hQ_u^{(2,3)} & -\alpha hQ_u^{(3,3)} \\ -\alpha(1 + hR_u^{(1)}) & hP_u^{(1,1)} & hQ_u^{(2,3)} & hQ_u^{(3,3)} \\ (h - \alpha)\bar{c}_u & 2h\beta M^{-1}(1,1)a_f & 2h\beta M^{-1}(1,1)b_f \end{bmatrix}^T, \quad (32)$$

$$X_{dyn,v} = \begin{bmatrix} (\alpha + hR_v^{(2)}) & -\alpha hP_v^{(2,2)} & -\alpha hP_v^{(2,3)} & -\alpha hP_v^{(3,2)} & -\alpha hP_v^{(3,3)} \\ -2\alpha hQ_v^{(1,2)} & -2\alpha hQ_v^{(1,3)} & -\alpha(1 + hR_v^{(2)}) & -\alpha hR_v^{(3)} & hP_v^{(2,2)} \\ hP_v^{(2,3)} & hP_v^{(3,2)} & hP_v^{(3,3)} & 2hQ_v^{(1,2)} & 2hQ_v^{(2,2)} & hR_v^{(2)} & hR_v^{(3)} & (h - \frac{d}{2})\bar{c}_v \\ \frac{d}{2}h\beta M^{-1}(2,3)(a_j^L - a_j^R) & \frac{d}{2}h\beta M^{-1}(2,3)(a_j^L + a_j^R) \\ \frac{d}{2}h\beta M^{-1}(2,3)(b_j^L - b_j^R) & \frac{d}{2}h\beta M^{-1}(2,3)(b_j^L + b_j^R) \end{bmatrix}^T, \quad (33)$$

$$X_{dyn,r} = \begin{bmatrix} (\alpha + hR_r^{(3)}) & -\alpha hP_r^{(2,2)} & -\alpha hP_r^{(2,3)} & -\alpha hP_r^{(3,2)} & -\alpha hP_r^{(3,3)} \\ -2\alpha hQ_r^{(1,2)} & -2\alpha hQ_r^{(1,3)} & -\alpha hR_r^{(2)} & -\alpha(1 + hR_r^{(3)}) & hP_r^{(2,2)} \\ hP_r^{(2,3)} & hP_r^{(3,2)} & hP_r^{(3,3)} & 2hQ_r^{(1,2)} & 2hQ_r^{(2,2)} & hR_r^{(2)} & hR_r^{(3)} & (h - \frac{d}{2})\bar{c}_r \end{bmatrix}^T$$

$$\begin{bmatrix} \frac{d}{2}h\beta M^{-1}(3,3)(a_j^L - a_j^R) & \frac{d}{2}h\beta M^{-1}(3,3)(a_j^L + a_j^R) \\ \frac{d}{2}h\beta M^{-1}(3,3)(b_j^L - b_j^R) & \frac{d}{2}h\beta M^{-1}(3,3)(b_j^L + b_j^R) \end{bmatrix}^T. \quad (34)$$

Proof. For a detailed breakdown of Proposition 3, including the values of $A_{dyn,j}(k)$ and $b_{dyn,j}(k)$ with $j \in \{u, v, r\}$, consult (Morel et al., 2024). \square

In the identification of the input gain considering the static model of the propellers, the regressors for each component of the velocity contained a different set of parameters and therefore the identification could be tackled in three independent steps. This is not exactly the case here. Observing, for instance, components 1 and 5 of the regressor $X_{dyn,u}$, it is easy to see that there are 2 unknowns $(\alpha, R_u^{(1)})$, since h is known. Hence, the value of α can be identified using just the regressor of the surge. However, from the components 1 and 8 of the regressor $X_{dyn,v}$, one can identify $(\alpha, R_v^{(3)})$, obtaining, possibly, a different value of α . Something similar happens with the regressor of the yaw. This problem does not occur with β , as it appears to always be coupled with other parameters that are different for each component of the velocity.

To solve this issue, there are different options. One possible option would consist in considering different dynamic models for each component, in other words, a different α_j for each $j \in \{u, v, r\}$. Although possible from a numerical perspective, this option does not look fully consistent with the underlying physics. Another option, the one implemented here, is to identify a unique α valid for all velocities. This implies solving an overdetermined system of equations, presented in 3, since there are more equations than unknowns in the regressors of the three velocities.

$$\begin{cases} X_{dyn,u}(1) = \alpha + hR_u^{(1)} \\ X_{dyn,u}(5) = -\alpha(1 + hR_u^{(1)}) \\ X_{dyn,v}(1) = \alpha + hR_v^{(2)} \\ X_{dyn,v}(8) = -\alpha(1 + hR_v^{(2)}) \\ X_{dyn,r}(1) = \alpha + hR_r^{(3)} \\ X_{dyn,r}(9) = -\alpha(1 + hR_r^{(3)}) \end{cases} \quad (35)$$

Remark 4. Please note that, with the proposed identification procedure considering dynamic propeller modelling, the value of some parameters related to the lumped disturbances, such as $P_u^{(1,1)}$, could have two different values. Although this is, of course, impossible, it is not particularly important since we are interested in identifying the input gain, which will be uniquely determined.

Once the parameters are identified, the input gain can be obtained. From the definition of the input gain in (11), using the force and torque in (13), and the first-order dynamic model of the thrusts in (15), the following dynamic model for the input gain is formulated as:

$$G_{dyn}(k) = hM^{-1}\alpha\tau(k-1) + hM^{-1}\beta\tau_{st}(k-1), \quad (36)$$

where $G_{dyn}(k) = [G_{dyn,u}(k), G_{dyn,v}(k), G_{dyn,r}(k)]^T$ and $\tau_{st}(k)$ is made up of the force F_u and torque τ_r given by (17) and (18), which turn out to be the static model equations for the force and torque. Subsequently, we can group the expression $hM^{-1}\tau(k-1)$ as $G_{dyn}(k-1)$. Taking advantage of this simplification, (36) becomes:

$$G_{dyn}(k) = \alpha G_{dyn}(k-1) + hM^{-1}\beta\tau_{st}(k-1), \quad (37)$$

which shows that the input gain allows now for a first-order dynamic model.

This sets the groundwork for applying the equation across all velocities, culminating in a comprehensive application of the dynamic model for input gain estimation as shown:

$$G_{dyn,u}(k) = \alpha G_{dyn,u}(k-1) + X_{dyn,u}(10)\left(\bar{\delta}(k-1)^2 + \frac{\Delta\delta(k-1)^2}{4}\right) + X_{dyn,u}(11)\bar{\delta}(k-1), \quad (38)$$

$$G_{dyn,p}(k) = \begin{cases} \alpha G_{dyn,p}(k-1) + X_{dyn,p}(19)\bar{\delta}(k-1)\Delta\delta(k-1) \\ + X_{dyn,p}(21)\frac{\Delta\delta(k-1)}{2}, & (f, f) \\ \alpha G_{dyn,p}(k-1) \pm X_{dyn,p}(18)\left(\bar{\delta}(k-1)^2 + \frac{\Delta\delta(k-1)^2}{4}\right) \\ + X_{dyn,p}(19)\bar{\delta}(k-1)\Delta\delta(k-1) \pm X_{dyn,p}(20)\bar{\delta}(k-1), & (f, r) \\ + X_{dyn,p}(21)\frac{\Delta\delta(k-1)}{2} \\ \alpha G_{dyn,p}(k-1) \pm X_{dyn,p}(18)\left(\bar{\delta}(k-1)^2 + \frac{\Delta\delta(k-1)^2}{4}\right) \\ + X_{dyn,p}(19)\bar{\delta}(k-1)\Delta\delta(k-1) \pm X_{dyn,p}(20)\bar{\delta}(k-1), & (r, f) \\ + X_{dyn,p}(21)\frac{\Delta\delta(k-1)}{2} \end{cases} \quad (39)$$

where $p \in \{v, r\}$.

Being a first-order model, the input gain cannot be computed only with the information of the PWM signals but also requires an initial condition. This initial condition is generally unknown. However, we can take advantage of the following property.

Property 1. Consider the evolution of the input gain given in (38)–(39). Then, provided that $\alpha < 1$, the value of the input gain at any instant k' sufficiently large mainly depends on the value of the PWM signals. In other words, the influence of the initial condition vanishes with time.

Proof. The proof is straightforward since the input gain is a first-order system with a transition matrix $\Phi(k) = \alpha^k$. Provided that $\alpha < 1$, the influence of the initial conditions vanishes as k increases. \square

Remark 5. The fact that $\alpha < 1$ could be inferred from the definition of the dynamic model for the thrust in (15) since otherwise the thrust could grow to infinity with zero input. However, without imposition, a suitable value of α is obtained with the proposed identification procedure, as shown in Section 6.

6. Identification experiments, results and discussion

In this section, the conducted experiments and the obtained results are presented and discussed. First, a detailed explanation of the experimental setup and the identification metrics used is provided. The identification results are then displayed using the second-order static model. The section concludes with the results obtained from the first-order dynamic model, including a discussion comparing both analysed models.

6.1. Experimental setup and identification metrics

The *Yellowfish* ASV was programmed to carry out a wide range of trajectories, divided into two main categories: forward and circular movements. The aim was to collect significant experimental data to excite the surge and yaw dynamics. In the case of forward movements, manoeuvres were performed using constant and variable forward velocities, as well as zigzag trajectories. Similarly, for circular movements, manoeuvres were designed to excite yaw dynamics at both constant and variable rates, also integrating movements with constant and variable forward velocity into the turns.

This extensive set of manoeuvres was intended to thoroughly evaluate the ASV performance in executing simple linear paths and complex navigational patterns. These manoeuvres produced a detailed dataset crucial for analysing and validating the navigational model, accurately reflecting the ASV real-world performance under a variety of controlled conditions.

The dataset was then strategically divided into two subsets: one devoted to the identification of the surge dynamics, whose points

correspond to those in which forward movements were performed, where both propellers are in the $\{f, f\}$ zone; and another one for the identification of the yaw and sway dynamics, including those points that correspond to circular movements, considering the $\{f, r\}$ and $\{r, f\}$ zones and always disregarding any point in the $\{r, r\}$ zone, as it will not be analysed in this identification process. Then, each subset is further divided into a training set and a validation set. The complete dataset, comprising 16,025 data points, with a higher concentration of data within the $\{f, r\}$ and $\{r, f\}$ zones compared to the $\{f, f\}$ zone, divided into 127 trajectory segments, resulting in 53.42 min of experiments, is available in Morel (2024).

The way in which the dataset is split into training and validation subsets is done in two different ways. First, all data points are randomly divided, according to a given percentage, into these two sets. The second option randomly divides the trajectory segments, so that some of them belong to the training dataset, and others to the validation dataset. Since the segments have a fixed number of data points, this partition will not achieve an exact division of the dataset in terms of a given percentage but will try to approximate it as much as possible. Table 3 presents the separation methods used, along with a description of each; Fig. 4 shows the field in which the experiments were conducted. It depicts a calm lake setting. Two paths are presented: one generated by the internal Navio2 GNSS and the other by the external GNSS, which is the one used for its higher satellite precision.

Regarding the values used for the validation analysis, the velocity values obtained by the data preparation process of the experimental results (v) are the ground truth and are compared to the velocities predicted with the identified parameters (\hat{v}).

Two well-known metrics are used for validation, the R^2 , or coefficient of determination, and the mean absolute error (MAE):

- The R^2 is a statistical measure that represents the proportion of variance in a dependent variable that is predictable from the independent variables. It provides an indication of how well the data points fit a model; the closer R^2 is to 1, the better the model explains the variability of the output in relation to the input variables. It is a measure commonly used in least-squares regressions (Cameron and Windmeijer, 1997).

For the problem at hand, this metric is computed as follows:

$$R_j^2 = 1 - \frac{\sum_{k=1}^n (v_j(k) - \hat{v}_j(k))^2}{\sum_{k=1}^n (v_j(k) - \bar{v}_j)^2}, \quad (40)$$

where $j \in \{u, v, r\}$ and n is the number of points of the validation set.

- The MAE is particularly effective for regressors that involve multiple parameters because it provides a straightforward measure of the average magnitude of errors without considering their direction, which makes it highly suitable for evaluating the performance of models in predicting a wide range of outcomes (Willmott and Matsuura, 2005). In this case, it is computed as:

$$MAE_j = \frac{1}{n} \sum_{k=1}^n |v_j(k) - \hat{v}_j(k)|. \quad (41)$$

6.2. Identification results for static propeller modelling

In the first analysis, the sensitivity of the identification results with respect to the partition of the data is studied. To do so, a fixed 70% of the dataset is used for training and the 30% left is used for validation. To analyse the sensitivity, 20 random partitions are made and, for each metric, the mean and Standard Deviation (SD) are computed. Table 4 presents the numerical results for the two partition methods.

From these data, two important conclusions can be drawn. First, the random partition in independent points renders slightly better results. But, most importantly, is the fact that the deviation is very small (much

Table 3
Description of data separation methods for training data.

Separation method	Description
By Segments	Random grouping of the complete segments.
By Independent Points	Random and independent selection of the individual data points.

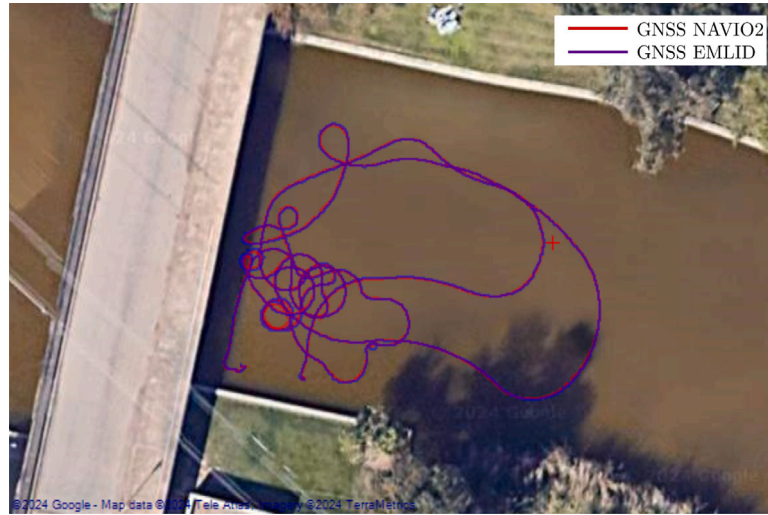


Fig. 4. The experiment field and ASV path.

Table 4
Comparison of MAE and R^2 metrics for different data separation methods using second-order static model.

	MAE _u	SD _u	MAE _v	SD _v	MAE _r	SD _r
By Segments	0.014377	2.9×10^{-3}	0.011913	6.2×10^{-4}	0.015895	2.1×10^{-3}
By Independent Points	0.011794	1.5×10^{-4}	0.011870	1.0×10^{-4}	0.015757	2.0×10^{-4}
	R^2_u	SD _u	R^2_v	SD _v	R^2_r	SD _r
By Segments	0.995708	2.3×10^{-3}	0.987277	1.8×10^{-3}	0.997468	1.2×10^{-3}
By Independent Points	0.997658	9.6×10^{-5}	0.987452	3.6×10^{-4}	0.997659	7.4×10^{-5}

Table 5
MAE values for different training percentages using second-order static model.

Training %	MAE _u	MAE _v	MAE _r	Validation %	MAE _u	MAE _v	MAE _r
70	0.012234	0.012666	0.013471	30	0.011092	0.010599	0.020743
60	0.013645	0.012879	0.014153	30	0.011370	0.010596	0.020164
50	0.016374	0.014090	0.014068	30	0.011580	0.010361	0.019268

smaller with independent points). This allows us to conclude that the way in which the data are partitioned does not have an important impact on the predictive capabilities of the identified model. This conclusion invites us to avoid the repetitions of the partitions in the rest of the analysis.

Attending to the quantitative values observed, the identified models show a really accurate prediction, in surge, sway, and yaw, with a determination coefficient always higher than 0.98.

In the next analysis, the sensitivity to the number of points in the training dataset is analysed. To do so, different percentages of points in the whole dataset are considered, with a constant keeping 30% for the validation dataset. The results are shown in [Tables 5](#) and [6](#).

With respect to the MAE, there is no significant change as the training dataset is reduced. This allows us to conclude that the performance of the model is consistent despite the reduction of data points.

Additionally, since a larger percentage of training might capture more variability and complexity, these results could suggest that the model is not overfitting to the training data. This is indicated by the fact that, in some cases, the MAE values for the validation set are lower

than those for the training set, implying that the model is not overly fine-tuned to the specific details of the training data.

Comparing the results using R^2 , a concordance with the obtained MAE values can be observed, allowing us to conclude that the model achieves a good level of prediction.

Finally, some graphical analysis are shown. Although the metrics provide very useful information, a graphical analysis allows us to understand the behaviour of the model, when it renders nice predictions, and when it fails. For this part, the dataset is partitioned in segments, this allowing us to observe dynamical behaviours.

As mentioned previously, the dataset was strategically divided into two subsets: one dedicated to surge dynamics and the other to yaw and sway dynamics. Consequently, the graphical representation of the surge results uses a different time window compared to those of sway and yaw, as they exhibit different movements.

[Fig. 5](#) shows three portions of the validation set, illustrating the estimated surge velocity during different manoeuvres, providing a wide range of velocity values, and the performance of the parameters obtained with the estimated velocity.

Table 6
 R^2 values for different training percentages using second-order static model.

Training %	R_u^2	R_v^2	R_r^2	Validation %	R_u^2	R_v^2	R_r^2
70	0.998177	0.984567	0.998602	30	0.987774	0.991418	0.992662
60	0.996305	0.985519	0.997190	30	0.987496	0.991008	0.992628
50	0.988801	0.982918	0.997262	30	0.987273	0.991643	0.993209

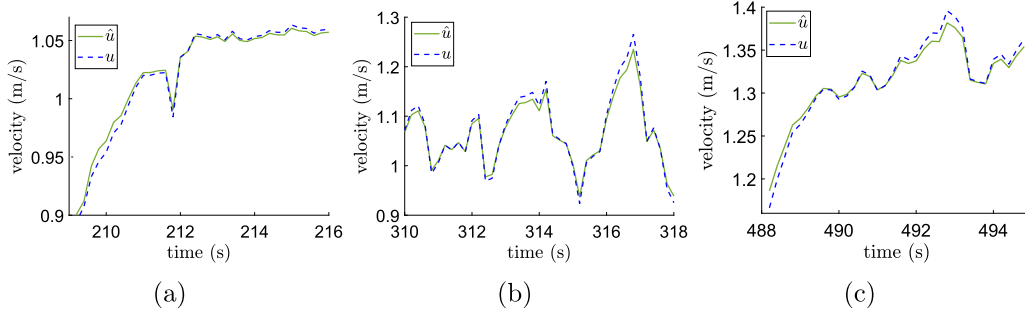


Fig. 5. Surge velocity u and estimated velocity \hat{u} in the validation subset using second-order static model.

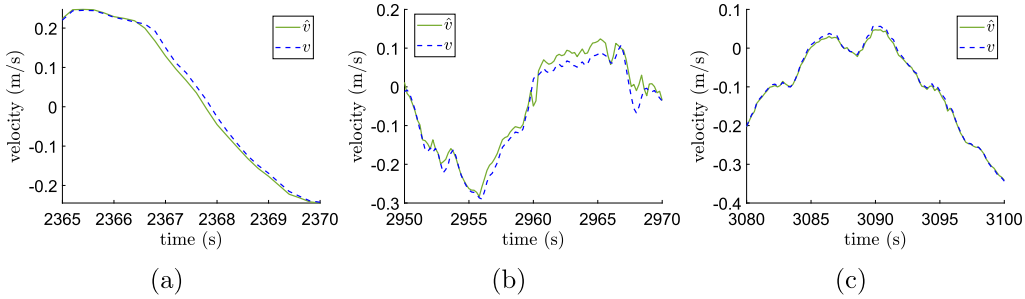


Fig. 6. Sway velocity v and estimated velocity \hat{v} in the validation subset using second-order static model.

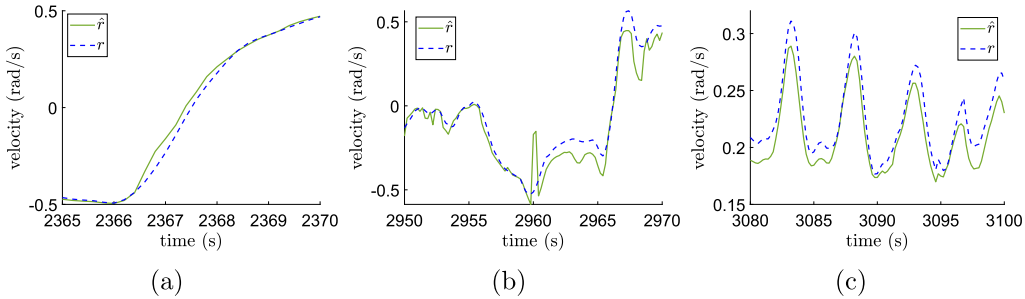


Fig. 7. Yaw rate r and estimated yaw rate \hat{r} in the validation subset using second-order static model.

Figs. 6 and 7 present the sway velocity and the yaw rate, respectively. In the yaw rate results, the zoomed-in section of the figure reveals that the estimated values do not reach the maximum levels during sharp turns. This can still be considered a valid response, as the experimental data used for this identification involved more abrupt movements than typical operations to capture the full range of the ASV movements.

Note that the time windows shown for the graphical results represent a small percentage of the total data obtained for the validation subset. Therefore, they should be considered alongside the previously stated numerical results, which describe the errors for the entire analysed dataset.

6.3. Identification results for dynamic propeller modelling

The same procedure is used to initially evaluate the mean values and standard deviation of 20 randomly grouped values and is applied

to the first-order dynamic model. However, in this case, since it is a dynamic model, the independent points take into account both the current values and those from the previous time step to estimate the next one. The results presented in Table 7 are quite positive and show very low standard deviation values. Consequently, for the subsequent analysis, only one group of values randomly grouped together will be examined.

In conducting the analysis to determine sensitivity to the number of points in the training dataset, Tables 8 and 9 present the MAE and R^2 results for the various percentages of points using the dynamic model.

Both the MAE and R^2 values show minimal fluctuation in the different percentages, demonstrating the consistent performance of the model. Compared to the dynamic model, it is evident that using a higher percentage of data for training produces consistently better results.

Observing the graphical analysis, the same time windows are used with identical training and validation datasets as for the previous model

Table 7Comparison of MAE and R^2 metrics for different data separation methods using first-order dynamic model.

	MAE_u	SD_u	MAE_v	SD_v	MAE_r	SD_r
By Segments	0.011628	1.2×10^{-3}	0.009654	6.3×10^{-4}	0.007861	5.5×10^{-4}
By Independent Points	0.011770	1.1×10^{-4}	0.009414	1.0×10^{-4}	0.007823	6.3×10^{-5}
	R^2_u	SD_u	R^2_v	SD_v	R^2_r	SD_r
By Segments	0.997505	1.5×10^{-3}	0.990236	1.5×10^{-3}	0.999523	1.8×10^{-4}
By Independent Points	0.997776	6.5×10^{-5}	0.991055	3.3×10^{-4}	0.999551	1.0×10^{-5}

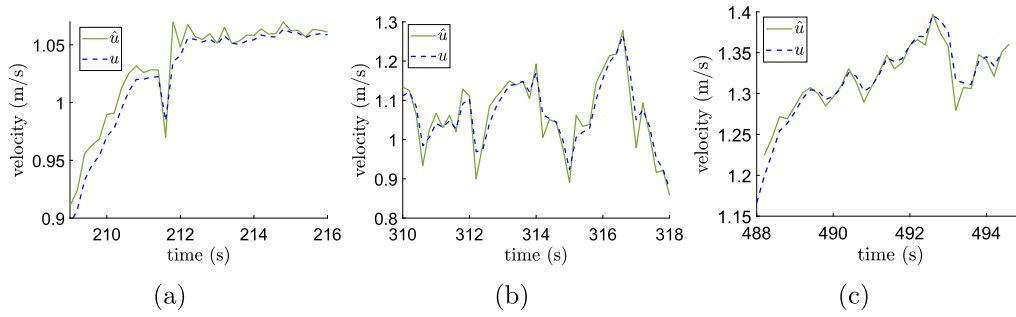
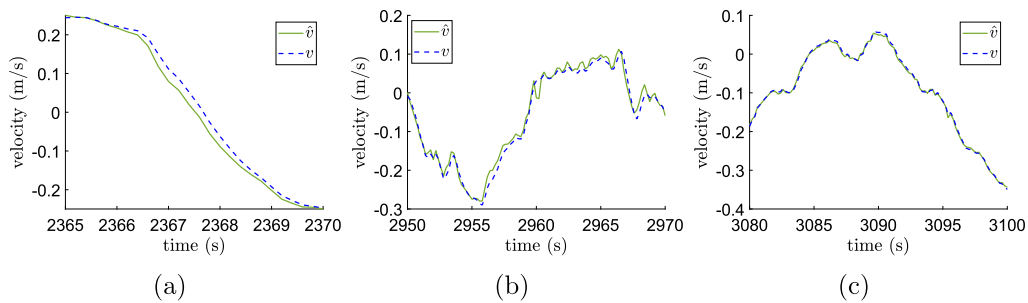
Table 8

MAE values for different training percentages using first-order dynamic model.

Training %	MAE_u	MAE_v	MAE_r	Validation %	MAE_u	MAE_v	MAE_r
70	0.011637	0.010785	0.008415	30	0.033513	0.007386	0.016770
60	0.012871	0.011076	0.008876	30	0.034702	0.008325	0.030219
50	0.015348	0.012492	0.008611	30	0.043901	0.008154	0.022668

Table 9 R^2 values for different training percentages using first-order dynamic model.

Training %	R^2_u	R^2_v	R^2_r	Validation %	R^2_u	R^2_v	R^2_r
70	0.998445	0.987943	0.999573	30	0.943559	0.996225	0.997599
60	0.996819	0.988532	0.999137	30	0.939760	0.995190	0.992966
50	0.989830	0.985986	0.999189	30	0.909676	0.995331	0.996110

**Fig. 8.** Surge velocity u and estimated velocity \hat{u} in the validation subset using first-order dynamic model.**Fig. 9.** Sway velocity v and estimated velocity \hat{v} in the validation subset using first-order dynamic model.

analysed. This approach enables a thorough comparison and evaluation of both models analysed in this section.

Fig. 8 displays the estimated surge velocity, and Figs. 9 and 10 show the results for sway velocity and yaw rate, respectively.

Regarding the surge results, the estimated values exhibit pronounced peaks and appear less smooth, as reflected in the metrics previously presented.

Considering sway velocity and yaw rate, the model demonstrates good and smooth tracking of the estimated velocities, although some peaks are more pronounced than those of the actual velocities, particularly in regions with abrupt velocity changes.

To obtain the estimated velocity values, it is necessary to determine the value of α using the identification equations for the three velocities 3. The resulting value of α is 0.998, which ensures the stability of the model, as discussed in Remark 5.

6.4. Discussion and comparison of the static and dynamic models

Finally, the differences between static and dynamic models are discussed. In particular, the first-order dynamic model produces superior results for the sway velocity and yaw rate, according to the metrics employed. Furthermore, graphical analysis shows improved accuracy in

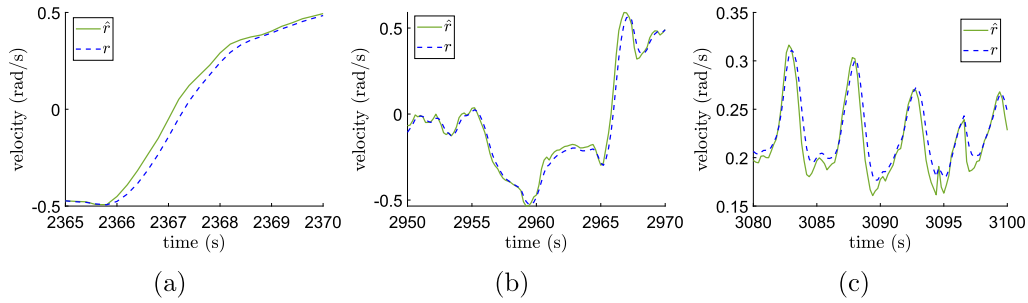


Fig. 10. Yaw rate r and estimated yaw rate \hat{r} in the validation subset using first-order dynamic model.

Table 10

Identified parameters and corresponding units of measurement used for the second-order static model.

Second-order static model						
Index	X_u	Unit	X_v	Unit	X_r	Unit
1	-0.0616	(m/s) ⁻¹	-0.0214	(m/s) ⁻¹	0.0424	(m/s) ⁻¹
2	0.0272	(m/s) ⁻¹	-0.0714	(m/s) ⁻¹	-0.1168	(m/s) ⁻¹
3	-0.0098	(m/s) ⁻¹	-0.0334	(m/s) ⁻¹	0.0369	(m/s) ⁻¹
4	0.0072	–	-0.0123	(m/s) ⁻¹	-0.0077	(m/s) ⁻¹
5	-0.0001	m/s	-0.0400	(m/s) ⁻¹	-0.0310	(m/s) ⁻¹
6	-0.0145	m/s	0.0329	(m/s) ⁻¹	-0.0931	(m/s) ⁻¹
7	0.1403	m/s	0.0407	–	0.0882	–
8			0.0334	–	-0.1505	–
9			-0.0018	m/s	0.0055	m/s
10			0.0092	m/s	-0.0872	m/s
11			-0.0381	m/s	-0.0743	m/s
12			-0.0032	m/s	0.0814	m/s
13			-0.0505	m/s	0.3206	m/s

Table 11

Identified parameters and corresponding units of measurement used for the first-order dynamic model.

First-order dynamic model parameters						
Index	$X_{u, dyn}$	Unit	$X_{v, dyn}$	Unit	$X_{r, dyn}$	Unit
1	0.8062	–	0.6904	–	0.9886	–
2	0.0893	(m/s) ⁻¹	-0.0091	(m/s) ⁻¹	0.0577	(m/s) ⁻¹
3	-0.1095	(m/s) ⁻¹	0.0237	(m/s) ⁻¹	0.1845	(m/s) ⁻¹
4	-0.0341	(m/s) ⁻¹	-0.0261	(m/s) ⁻¹	-0.0190	(m/s) ⁻¹
5	-0.7725	–	-0.0005	(m/s) ⁻¹	-0.0054	(m/s) ⁻¹
6	-0.1395	(m/s) ⁻¹	0.4328	(m/s) ⁻¹	0.0667	(m/s) ⁻¹
7	0.1622	(m/s) ⁻¹	0.3075	(m/s) ⁻¹	-0.0020	(m/s) ⁻¹
8	0.0301	(m/s) ⁻¹	-0.6978	–	-0.2723	–
9	0.0016	m/s	-0.1285	–	-1.0430	–
10	-0.0106	m/s	-0.0085	(m/s) ⁻¹	-0.1305	(m/s) ⁻¹
11	0.0611	m/s	-0.0494	(m/s) ⁻¹	-0.2120	(m/s) ⁻¹
12			0.0081	(m/s) ⁻¹	-0.0059	(m/s) ⁻¹
13			0.0004	(m/s) ⁻¹	0.0577	(m/s) ⁻¹
14			-0.4353	(m/s) ⁻¹	-0.1116	(m/s) ⁻¹
15			-0.3078	(m/s) ⁻¹	0.0358	(m/s) ⁻¹
16			0.1478	–	0.3419	–
17			-0.0007	m/s	-0.0013	m/s
18			-0.007	m/s	-0.0422	m/s
19			-0.007	m/s	-0.0385	m/s
20			0.0101	m/s	0.0394	m/s
21			-0.0214	m/s	0.0168	m/s

the estimated yaw rate, particularly in sharper curves, although some minor peaks persist compared to the second-order model.

In contrast, the surge velocity shows better results when using the static model. To understand this difference, it is important to note that the dataset used to identify the surge dynamics parameters is smaller than that for the sway and yaw. Furthermore, in the dynamic model, a single value of α is applied at all three velocities, which seems to favour the dynamics of the sway and yaw.

The static and dynamic models perform well, with the dynamic model offering slightly better results; however, it is more complex to implement and requires the stability of the dynamic model of the propellers (with $\alpha < 1$). Therefore, choosing which model to use ultimately depends on the preference and requirements of the user.

To conclude, Tables 10 and 11 present the values of the parameters identified for the static second-order model, as well as the values obtained using the dynamic first-order model.

The tables highlight the values required for the input gain equations presented in (23) and (28), using the vessel *Yellowfish*, where the dynamic model also incorporates the previously mentioned α value. All identified parameter values are presented to enable replication of the results.

7. Conclusions

This work presents a parameter identification methodology to determine the input gain of an ASV with fully unknown coefficients. The

unknown model parameters can be estimated through position and heading measurements, thus eliminating the need for acceleration data.

This study presents a practical method for jointly identifying the propeller model and the inertia matrix of an ASV, which means the effect of the propellers on its motion. The identification method included, with experimental results, both a second-order static model and a first-order dynamic model for the actuation system.

The models were applied to obtain the parameters of the *Yellowfish* ASV, with significant emphasis on experimental data acquisition to ensure robust parameter functionality across a significant operational range.

The effectiveness of the proposed methods is validated by applying identification metrics to the results, also allowing comparison between different models. For the second-order static model, a determination coefficient greater than 0.98 was achieved for surge velocity, sway velocity, and yaw rate. In contrast, when applying the first-order dynamic model to the same experimental data, the results yielded a range of 0.94 to 0.99 across all three velocities. These consistent values highlight the reliability and effectiveness of the models in accurately capturing vessel dynamics.

Furthermore, the importance of replicating the results is demonstrated, as it contributes to a deeper understanding of the models. To support this, the identified values obtained are reported in Tables 10 and 11, and all experimental data related to this work are available from Morel (2024).

CRedit authorship contribution statement

Thalia Morel: Writing – original draft, Visualization, Validation, Software, Investigation, Data curation. **Luis Orihuela:** Writing – review & editing, Writing – original draft, Visualization, Supervision, Software, Investigation, Formal analysis, Conceptualization. **Christophe Combastel:** Writing – review & editing, Visualization, Validation, Supervision, Investigation, Formal analysis. **Guillermo Bejarano:** Writing – review & editing, Writing – original draft, Visualization, Supervision, Resources, Methodology, Investigation, Funding acquisition.

Declaration of competing interest

The authors declare that they have no known competing financial interests or personal relationships that could have appeared to influence the work reported in this paper.

Acknowledgements

This work was supported by the Agencia Estatal de Investigación (AEI) through the Project AQUATRONIC under Grant PID2021 126921OA-C22, and through the Project ECOPORT under Grant TED2021-131326A-C22. We also thank the Consejería de Fomento, Infraestructuras y Ordenación del Territorio of the Junta de Andalucía for their collaboration and support in conducting tests in the Parque del Alamillo.

References

- Abrougui, H., Nejim, S., Hachicha, S., Zaoui, C., Dallagi, H., 2021. Modeling, parameter identification, guidance and control of an unmanned surface vehicle with experimental results. *Ocean Eng.* 241, 110038. <http://dx.doi.org/10.1016/j.oceaneng.2021.110038>, Elsevier.
- Alves, J., Oliveira, P., Oliveira, R., Pascoal, A., Rufino, M., Sebastiao, L., Silvestre, C., 2006. Vehicle and mission control of the DELFIM autonomous surface craft. In: 2006 14th Mediterr. Conf. Control Autom. IEEE., pp. 1–6. <http://dx.doi.org/10.1109/MED.2006.328689>.
- Blanke, M., Lindgaard, K.-P., Fossen, T.I., 2000. Dynamic model for thrust generation of marine propellers. *IFAC Proc.* 33 (21), 353–358. [http://dx.doi.org/10.1016/S1474-6670\(17\)37100-8](http://dx.doi.org/10.1016/S1474-6670(17)37100-8).
- Breivik, M., 2010. *Topics in Guided Motion Control of Marine Vehicles* (Ph.D. dissertation). Norwegian Univ. of Science and Technology.
- Caccia, M., Bibuli, M., Bono, R., Bruzzone, G., Bruzzone, G., Spirandelli, E., 2007. Unmanned surface vehicle for coastal and protected waters applications: The charlie project. *Mar. Technol. Soc. J.* 41 (2), 62–71. <http://dx.doi.org/10.4031/002533207787442259>, Marine Technology Society.
- Caccia, M., Bruzzone, G., Bono, R., 2008. A practical approach to modeling and identification of small autonomous surface craft. *IEEE J. Ocean. Eng.* 33 (2), 133–145. <http://dx.doi.org/10.1109/JOE.2008.920157>, IEEE.
- Cameron, A.C., Windmeijer, F.A.G., 1997. An R-squared measure of goodness of fit for some common nonlinear regression models. *J. Econom.* 77 (2), 329–342. [http://dx.doi.org/10.1016/S0304-4076\(96\)01818-0](http://dx.doi.org/10.1016/S0304-4076(96)01818-0), Elsevier.
- Curcio, J., Leonard, J., Patrikalakis, A., 2005. SCOUT-a low cost autonomous surface platform for research in cooperative autonomy. In: *Proc. of OCEANS 2005 MTS/IEEE*. IEEE, pp. 725–729. <http://dx.doi.org/10.1109/OCEANS.2005.1639838>.
- Eriksen, B.-O.H., Breivik, M., 2017. Modeling, identification and control of high-speed ASVs: Theory and experiments. In: *Sens. Control Auton. Veh. Appl. Land Water Air Veh.* Springer Int. Publ., Cham, pp. 407–431. http://dx.doi.org/10.1007/978-3-319-55372-6_19.
- Fossen, T.I., 2011. *Handbook of Marine Craft Hydrodynamics and Motion Control*. John Wiley & Sons, London, U.K.
- Gantiva Osorio, M.E., Ierardi, C., Jurado Flores, I., Pereira Martín, M., Millán Gata, P., 2024. Coordinated control of multiple autonomous surface vehicles: Challenges and advances — A systematic review. *Ocean Eng.* 312, 119160. <http://dx.doi.org/10.1016/j.oceaneng.2024.119160>.
- Gantiva Osorio, M.E., Millán Gata, P., Bejarano Pellicer, G., 2024. Implementation and evaluation of state observers and motion controllers in autonomous surface vehicle. *Instrum. Viewp.* (23), 16–17, SARTI. [Online]. Available: <http://hdl.handle.net/2117/411432>.
- Jovanović, I., Perčić, M., BahooToroody, A., Fan, A., Vladimir, N., 2024. Review of research progress of autonomous and unmanned shipping and identification of future research directions. *J. Mar. Eng. Technol.* 23 (2), 82–97, Taylor & Francis.
- Liu, L., Wang, D., Peng, Z., 2019. State recovery and disturbance estimation of unmanned surface vehicles based on nonlinear extended state observers. *Ocean Eng.* 171, 625–632. <http://dx.doi.org/10.1016/j.oceaneng.2018.11.008>, Elsevier.
- Majroh, J., Buch, T., 2006. Modelling, simulation and control of an autonomous surface marine vehicle for surveying applications Measuring Dolphin MESSIN. In: *Adv. Unmanned Mar. Veh., Inst. Eng. Technol.* In: Control, Robotics and Sensors series, pp. 329–352. http://dx.doi.org/10.1049/PBCE069E_ch16.
- Morel, T., 2024. Dataset for identification of the yellowfish ASV. Mendeley Data, V1. <http://dx.doi.org/10.17632/zhtc73r8bt.1>.
- Morel, T.A., Bejarano, G., Manzano, J.M., Orihuela, L., 2022a. Experimental validation of robust non-linear state observers for autonomous surface vehicles equipped with position sensors. In: 2022 IEEE Conf. Control Technol. Appl. CCTA, IEEE, pp. 357–362. <http://dx.doi.org/10.1109/CCTA49430.2022.9966024>.
- Morel, T.A., Manzano, J.M., Bejarano, G., Orihuela, L., et al., 2022b. Modelling and Identification of an Autonomous Surface Vehicle: Technical Report. Tech. Rep., Universidad Loyola Andalucía, <http://hdl.handle.net/20.500.12412/3270>.
- Morel, T., Orihuela, L., Combastel, C., Bejarano, G., 2024. Practical identification approach for the actuation dynamics of autonomous surface vehicles with minimal instrumentation: extended version. <http://dx.doi.org/10.48550/arXiv.2410.00631>, arXiv preprint [arXiv:2410.00631](https://arxiv.org/abs/2410.00631).
- Morel, T.A., Orihuela Espina, L., Bejarano Pellicer, G., 2023. Modelling and identification of an autonomous surface vehicle. *Instrum. Viewp.* (22), 32–33, [Online]. URL: <http://hdl.handle.net/20.500.12412/3270>.
- Mu, D., Wang, G., Fan, Y., Sun, X., Qiu, B., 1989. Modeling and identification for vector propulsion of an unmanned surface vehicle: Three degrees of freedom model and response model. *Sensors* 18, 2018. <http://dx.doi.org/10.3390/s18061889>.
- Peng, Z., Liu, L., Wang, J., 2021. Output-feedback flocking control of multiple autonomous surface vehicles based on data-driven adaptive extended state observers. *IEEE Trans. Cybern.* 51 (9), 4611–4622. <http://dx.doi.org/10.1109/TCYB.2020.3009992>.
- Peng, Z., Wang, J., Wang, D., Han, Q.-L., 2020. An overview of recent advances in coordinated control of multiple autonomous surface vehicles. *IEEE Trans. Inform.* 17 (2), 732–745. <http://dx.doi.org/10.1109/TII.2020.3004343>, IEEE.
- Savitzky, A., Golay, M.J.E., 1964. Smoothing and differentiation of data by simplified least squares procedures. *Anal. Chem.* 36 (8), 1627–1639. <http://dx.doi.org/10.1021/ac60214a047>.
- Simetti, E., Indiveri, G., 2022. Control oriented modeling of a twin thruster autonomous surface vehicle. *Ocean Eng.* 243, 110260. <http://dx.doi.org/10.1016/j.oceaneng.2021.110260>, Elsevier.
- Simmons, B.M., 2021. System identification for propellers at high incidence angles. *J. Aircr.* 58 (6), 1336–1350. <http://dx.doi.org/10.2514/1.C036329>.
- Sonnenburg, C.R., Woolsey, C.A., 2013. Modeling and identification, and control of an unmanned surface vehicle. *J. Field Robot.* 30 (3), 371–398. <http://dx.doi.org/10.1002/rob.21452>.
- The Society of Naval Architecture and Marine Engineers, 1950. *Nomenclature For Treating the Motion of a Submerged Body Through a Fluid*. Tech. Res. Bull. No. 1–5.

- Willmott, C.J., Matsuura, K., 2005. Advantages of the mean absolute error (MAE) over the root mean square error (RMSE) in assessing average model performance. *Clim. Res.* 30 (1), 79–82.
- Wu, G., Zhang, J., Li, G., Wang, L., Yu, Q., Guo, J., 2022. Identification method of nonlinear maneuver model for unmanned surface vehicle from sea trial data based on support vector machine. *J. Mech. Sci. Technol.* 36 (8), 4257–4267. <http://dx.doi.org/10.1007/s12206-022-0743-0>, Springer.
- Xu, P.-F., Cheng, C., Cheng, H.-X., Shen, Y.-L., Ding, Y.-X., 2020. Identification-based 3 DOF model of unmanned surface vehicle using support vector machines enhanced by cuckoo search algorithm. *Ocean Eng.* 197, 106898. <http://dx.doi.org/10.1016/j.oceaneng.2019.106898>, Elsevier.
- Zuev, A., Zhirabok, A., Filaretov, V., 2020. Fault identification in underwater vehicle thrusters via sliding mode observers. *Int. J. Appl. Math. Comput. Sci.* 30 (4), 679–688. <http://dx.doi.org/10.34768/amcs-2020-0050>.